energies

MDPI

Article

Gas-Path Health Estimation for an Aircraft Engine Based on a Sliding Mode Observer

Xiaodong Chang, Jinquan Huang *, Feng Lu and Haobo Sun

College of Energy and Power Engineering, Nanjing University of Aeronautics and Astronautics, 29 Yudao Road, Nanjing 210016, China; cxd18762406179@163.com (X.C.); lufengnuaa@126.com (F.L.); shb186024@163.com (H.S.)
* Correspondence: jhuang@nuaa.edu.cn; Tel.: +86-139-5179-6358

Academic Editor: Chang Sik Lee
Received: 7 June 2016; Accepted: 21 July 2016; Published: 29 July 2016

Abstract: Aircraft engine gas-path health monitoring (GPHM) plays a critical role in engine health management (EHM). Among model-based approaches, the Kalman filter (KF) has been widely employed in GPHM. The main shortcoming of KF-based scheme lies in the lack of robustness against uncertainties. To enhance robustness, this paper describes a new GPHM architecture using a sliding mode observer (SMO). The convergence of the error system in uncertainty-existing circumstances is demonstrated, and the proposed method is developed to estimate components' performance degradations regardless of modeling uncertainties. Simulations using a nonlinear model of a turbofan engine are presented, in which health monitoring problems are handled by the KF and the SMO, respectively. Results indicate the proposed approach possesses better diagnostic performance compared to the KF-based scheme, and the SMO shows its strong robustness and great potential to be applied to GPHM.

Keywords: aircraft engines; health estimation; modeling uncertainties; sliding mode observer (SMO); linear matrix inequalities (LMIs)

1. Introduction

Modern aircraft gas turbine engines are extremely complex systems that are subjected to extreme conditions. Over repeated flight cycles, the lifespan of engine components will be affected, and malfunctions may occur [1]. An aircraft engine will exhibit gradual degradation in the gas path over its operating life [2]. This is usually caused by the fouling or erosion that happens to compressors or turbines as parts wear from regular use. Generally these deteriorations are reflected by variations of components' efficiencies and flow capacities, which are the so-called "health parameters". Health parameters are not directly measureable, but their degradations cause changes in other observable parameters, such as temperature, pressure and rotational speed. The health degradation estimation plays a critical role in engine gas path health management system, which provides an evaluation of components' performance based on the level of degradation of efficiencies and flow capacities, and helps operators determine a regular maintenance schedule and arrange replacement of components when the performance reaches unacceptable levels.

Several approaches have been introduced to estimate the health condition of gas-path components, which can be classified into two types: model-based methods (such as observers and filters) and data-based methods (such as fuzzy logic, neural networks and genetic algorithms). Compared to data-based approaches, model-based approaches utilize all model information available, and offer better estimation accuracy [3]. A well-developed model-based strategy for health monitoring systems is the Kalman filter (KF) strategy. Luppold et al. [4] proposed an algorithm based on a KF concept to estimate in-flight engine performance variations. Simon et al. [5] applied the constrained KF approach, along with constraint tuning on the basis of measurement residuals, to estimate engine

health parameters. Since piecewise-linear models are linearized from a component-level model (CLM), which is a complex nonlinear representation of the gas turbine engine, modeling errors that decrease the accuracy of the health estimation are inevitable. In view of this, Brotherton presented an approach that fused a physical model called self-tuning on-board real-time model (STORM) with an empirical neural net model to provide a unique hybrid model (eSTORM) base on a KF, aiming to compensate modeling errors and provide engine diagnostics [6]. Volponi et al. [7] further developed eSTORM, by providing a self-tuning technique to the engine model as the engine evolved over the course of its life, to ensure accurate performance tracking.

Sliding mode observer (SMO) techniques have gained lots of attention in recent years. One of the reasons is due to their robustness against modeling uncertainties. As any model is unable to perfectly represent the system, robust state estimation is a vital property for the accuracy of state monitoring systems. Edwards et al. [8] proposed the architecture for fault detection and isolation (FDI) via sliding mode techniques. Ng at al. [9] presented a disturbance decoupled fault reconstruction approach focused on actuator faults. Tan et al. [10] reported the application of SMOs in sensor fault reconstruction. Alwi et al. [11] described a sliding mode fault reconstruction scheme based on a linear parameter varying model for an aircraft benchmark problem, to deal with aircraft sensor faults considering uncertainties and disturbances. Rahme et al. [12] proposed an adaptive SMO approach to diagnose sensor faults of gas turbines, where the degradations of health parameters are treated as constant uncertainties. So far uses of SMO in fault detection have mainly been in handling actuator/sensor fault cases, and to the authors' knowledge, research has barely been done on the application of the sliding mode technique to engine health performance monitoring systems.

In this paper, an SMO-based health monitoring scheme for an aircraft engine is proposed. With health parameters treated as state variables, a robust SMO is developed to estimate the degradations of health parameters, despite the existence of modeling uncertainties. The convergence of the error system in uncertainty-existing circumstances is demonstrated. Once sliding motion is achieved, the system is independent of the uncertainties due to the so-called equivalent output error injection term. Simulations show that in comparison with the KF scheme, the proposed SMO has better diagnostic performance in engine health degradation estimation.

2. Theory and Modeling

2.1. Modeling and Preliminaries

Since the proposed SMO is a kind of model-based algorithm, a linear state variable model (SVM) is required, which is a representative of the engine dynamic nonlinear model in a small range around the steady-state operating point. The linear model of an aircraft engine is as follows:

$$\begin{aligned} \dot{\boldsymbol{x}}(t) &= \boldsymbol{A}\boldsymbol{x}(t) + \boldsymbol{B}\boldsymbol{u}(t) + \boldsymbol{L}\boldsymbol{h}(t) \\ \boldsymbol{y}(t) &= \boldsymbol{C}\boldsymbol{x}(t) + \boldsymbol{D}\boldsymbol{u}(t) + \boldsymbol{M}\boldsymbol{h}(t) \end{aligned} \tag{1}$$

where $\boldsymbol{x}$ is the state vector, $\boldsymbol{u}$ is the input, $\boldsymbol{y}$ is the measurable output, and h is the health parameter vector. $\boldsymbol{A}$, $\boldsymbol{B}$, $\boldsymbol{C}$, $\boldsymbol{D}$, $\boldsymbol{L}$ and $\boldsymbol{M}$ are corresponding coefficient matrices. All variables in the linear model are normalized. The linear engine model is extracted from the CLM, which is a nonlinear dynamical representative of a real engine. The commonly used linearization methods for establishing engine SVM include the bias derivative method [13] and fitting method [14–16]. Compared to the bias derivative method, the fitting method is more feasible in low-order systems, and it possesses a higher modeling precision [14]. In this paper an improved least square fitting method is adopted to construct the engine SVM in Equation (1). To solve the initial value problem in fitting method, the initial values of coefficient matrices are obtained by the bias derivative method to create an initial linear model. Then the coefficient matrices are optimized by fitting the simulation data generated by the initial linear model and dynamic simulation data from the CLM [15]. The modeling method was verified in [15] and showed a satisfactory accuracy to be employed in model-based monitoring systems.

In order to estimate health parameters via observer techniques, health parameters is required to be considered as state variables, thus the following augmented system is created:

$$\begin{aligned} \begin{bmatrix} \dot{\boldsymbol{x}}(t) \\ \dot{\boldsymbol{h}}(t) \end{bmatrix} &= \begin{bmatrix} \boldsymbol{A} & \boldsymbol{L} \\ \boldsymbol{0} & \boldsymbol{0} \end{bmatrix} \begin{bmatrix} \boldsymbol{x}(t) \\ \boldsymbol{h}(t) \end{bmatrix} + \begin{bmatrix} \boldsymbol{B} \\ \boldsymbol{0} \end{bmatrix} \boldsymbol{u}(t) \\ \boldsymbol{y}(t) &= \begin{bmatrix} \boldsymbol{C} & \boldsymbol{M} \end{bmatrix} \begin{bmatrix} \boldsymbol{x}(t) \\ \boldsymbol{h}(t) \end{bmatrix} + \boldsymbol{D}\boldsymbol{u}(t) \end{aligned} \tag{2}$$

For analysis convenience Equation (2) can be presented as:

$$\begin{aligned} \dot{\boldsymbol{x}}_a(t) &= \boldsymbol{A}_a\boldsymbol{x}_a(t) + \boldsymbol{B}_a\boldsymbol{u}(t) \\ \boldsymbol{y}(t) &= \boldsymbol{C}_a\boldsymbol{x}_a(t) + \boldsymbol{D}_a\boldsymbol{u}(t) \end{aligned} \tag{3}$$

where $\boldsymbol{A}_a \in \mathbb{R}^{n\times n}$, $\boldsymbol{B}_a \in \mathbb{R}^{n\times m}$, $\boldsymbol{C}_a \in \mathbb{R}^{p\times n}$, $\boldsymbol{D}_a \in \mathbb{R}^{p\times m}$. In Equation (3), the information of health parameters are all in $\boldsymbol{x}_a(t)$, thus it's possible to estimate health degradation via an observer.

A change of coordinates is introduced to simplify the observer designing process. The coordinate transformation is associated with the invertible matrix:

$$\boldsymbol{T}_c = \begin{bmatrix} \boldsymbol{N}_c^T \\ \boldsymbol{C}_a \end{bmatrix} \tag{4}$$

where $\boldsymbol{N}_c \in \mathbb{R}^{n\times(n-p)}$ spans the null-space of $\boldsymbol{C}_a$. With the transformation, the measurement matrix has the form:

$$\boldsymbol{C}_c = \boldsymbol{C}_a\boldsymbol{T}_c^{-1} = \begin{bmatrix} \boldsymbol{0} & \boldsymbol{I}_p \end{bmatrix} \tag{5}$$

where $\boldsymbol{I}_c \in \mathbb{R}^{p\times p}$ denotes the identity matrix. In the new coordinates, Equation (3) can be described as:

$$\begin{aligned} \dot{\boldsymbol{x}}_c(t) &= \boldsymbol{A}_c\boldsymbol{x}_c(t) + \boldsymbol{B}_c\boldsymbol{u}(t) \\ \boldsymbol{y}(t) &= \boldsymbol{C}_c\boldsymbol{x}_c(t) + \boldsymbol{D}_c\boldsymbol{u}(t) \end{aligned} \tag{6}$$

where $\boldsymbol{x}_c(t) = \boldsymbol{T}_c\boldsymbol{x}_a(t)$, $\boldsymbol{A}_c = \boldsymbol{T}_c\boldsymbol{A}_a{\boldsymbol{T}_c}^{-1}$, $\boldsymbol{B}_c = \boldsymbol{T}_c\boldsymbol{B}_a$, and $\boldsymbol{D}_c = \boldsymbol{D}_a$. $\boldsymbol{A}_c$ is in the form of $\begin{bmatrix} \boldsymbol{A}_{c11} & \boldsymbol{A}_{c12} \\ \boldsymbol{A}_{c21} & \boldsymbol{A}_{c22} \end{bmatrix}$ where $\boldsymbol{A}_{c11} \in \mathbb{R}^{(n-p)\times(n-p)}$.

In order to exploit the robustness of SMO, Equation (6) is added with modeling uncertainties as follows:

$$\begin{aligned} \dot{\boldsymbol{x}}_c(t) &= \boldsymbol{A}_c\boldsymbol{x}_c(t) + \boldsymbol{B}_c\boldsymbol{u}(t) + \boldsymbol{Q}_c\xi(t,\boldsymbol{x},\boldsymbol{u}) \\ \boldsymbol{y}(t) &= \boldsymbol{C}_c\boldsymbol{x}_c(t) + \boldsymbol{D}_c\boldsymbol{u}(t) \end{aligned} \tag{7}$$

where $\boldsymbol{Q}_c \in \mathbb{R}^{n\times h}$ represents the uncertainty distribution matrix. $\xi(t,\boldsymbol{x},\boldsymbol{u}) \in \mathbb{R}^h$ denotes uncertainties, which are unknown but bounded:

$$||\,\xi(t,\boldsymbol{x},\boldsymbol{u})\,|| < \beta \tag{8}$$

where β is a known real scalar. The notation $||\cdot||$ represents the Euclidean norm for vectors and the induced spectral norm for matrices.

2.2. Sliding Mode Observer-Based Gas-Path Health Monitoring Architecture

In this sub-section, a SMO is designed to fulfill robust degrading estimation based on Equation (7). Define $\boldsymbol{e}_y(t) = \hat{\boldsymbol{y}}(t) - \boldsymbol{y}(t)$ as output estimation error. Consider a SMO of the form:

$$\begin{aligned} \dot{\hat{\boldsymbol{x}}}_c(t) &= \boldsymbol{A}_c\hat{\boldsymbol{x}}_c(t) + \boldsymbol{B}_c\boldsymbol{u}(t) - \boldsymbol{G}_l\boldsymbol{e}_y(t) + \boldsymbol{G}_n\boldsymbol{v}(t) \\ \hat{\boldsymbol{y}}(t) &= \boldsymbol{C}_c\hat{\boldsymbol{x}}_c(t) + \boldsymbol{D}_c\boldsymbol{u}(t) \end{aligned} \tag{9}$$

where $(\hat{\boldsymbol{x}}_c, \hat{\boldsymbol{y}})$ are the estimates of $(\boldsymbol{x}_c, \boldsymbol{y})$. $\boldsymbol{G}_l \in \mathbb{R}^{n\times p}$, $\boldsymbol{G}_n \in \mathbb{R}^{n\times p}$ are the linear gain matrix and the nonlinear gain matrix, respectively. $v(t) \in \mathbb{R}^{p}$ is defined as:

$$\boldsymbol{\nu}(t) = \begin{cases} -\rho \frac{\boldsymbol{P}_0 \boldsymbol{e}_y(t)}{||\boldsymbol{P}_0 \boldsymbol{e}_y(t)||} & \boldsymbol{e}_y(t) \neq 0 \\ 0 & \text{otherwise} \end{cases} \tag{10}$$

where ρ is a positive real scalar. $\boldsymbol{P}_0 \in \mathbb{R}^{p\times p}$ is a symmetric positive matrix that will be defined later. $\boldsymbol{G}_n$ is designed to be in the structure:

$$\boldsymbol{G}_n = \begin{bmatrix} -\boldsymbol{E} \\ \boldsymbol{I}_p \end{bmatrix} \tag{11}$$

where $\boldsymbol{E} \in \mathbb{R}^{(n-p)\times p}$ represents the design freedom, and no special structure is imposed on G_l.

Define $\boldsymbol{e}(t) = \hat{\boldsymbol{x}}_c(t) - \boldsymbol{x}_c(t)$ as state estimation error. The following error system is obtained from Equations (7) and (9):

$$\dot{\boldsymbol{e}}(t) = (\boldsymbol{A}_c - \boldsymbol{G}_l \boldsymbol{C}_c)\boldsymbol{e}(t) + \boldsymbol{G}_n \boldsymbol{\nu}(t) - \boldsymbol{Q}_c \xi(t, \boldsymbol{x}, \boldsymbol{u}) \tag{12}$$

where $\boldsymbol{e}_y(t)$ is replaced considering that $\boldsymbol{e}_y(t) = \boldsymbol{C}_c \boldsymbol{e}(t)$. Due to the structure of $\boldsymbol{C}_c$, $\boldsymbol{e}_y(t)$ is directly extracted from the last p components of $\boldsymbol{e}(t)$, which means the last p components of $\boldsymbol{e}(t)$ are $\boldsymbol{e}_y(t)$, i.e., $\boldsymbol{e} = \left(\boldsymbol{e}_1^T, \boldsymbol{e}_y^T\right)^T$ where $\boldsymbol{e}_1 \in \mathbb{R}^{n-p}$. Define $\boldsymbol{A}_p = \boldsymbol{A}_c - \boldsymbol{G}_l \boldsymbol{C}_c$, in the form of $\begin{bmatrix} \boldsymbol{A}_{p11} & \boldsymbol{A}_{p12} \\ \boldsymbol{A}_{p21} & \boldsymbol{A}_{p22} \end{bmatrix}$ where $\boldsymbol{A}_{p11} \in \mathbb{R}^{(n-p)\times(n-p)}$. Then the error system can be partitioned as:

$$\begin{aligned} \dot{\boldsymbol{e}}_1(t) &= \boldsymbol{A}_{p11}\boldsymbol{e}_1(t) + \boldsymbol{A}_{p12}\boldsymbol{e}_y(t) - \boldsymbol{E}\boldsymbol{\nu}(t) - \boldsymbol{Q}_{c1}\xi(t, \boldsymbol{x}, \boldsymbol{u}) \\ \dot{\boldsymbol{e}}_y(t) &= \boldsymbol{A}_{p21}\boldsymbol{e}_1(t) + \boldsymbol{A}_{p22}\boldsymbol{e}_y(t) + \boldsymbol{\nu}(t) - \boldsymbol{Q}_{c2}\xi(t, \boldsymbol{x}, \boldsymbol{u}) \end{aligned} \tag{13}$$

where $\boldsymbol{Q}_{c1} \in \mathbb{R}^{(n-p)\times h}$ and $\boldsymbol{Q}_{c2} \in \mathbb{R}^{p\times h}$.

Define a sliding surface:

$$S = \{\boldsymbol{e} \mid \boldsymbol{C}_c \boldsymbol{e} = 0\} \tag{14}$$

In order to guarantee the stability of the observer, it is required to prove that the error system can be driven to the sliding surface in finite time and remained on it by appropriate design. In view of this, the following conclusion is presented.

Theorem 1: Considering the error in Equation (12), with $\mathbf{G}_n$ in the structure of Equation (11), assume that there exists a matrix $\boldsymbol{G}_l$ and a Lyapunov matrix $\boldsymbol{P}$ of the form:

$$\boldsymbol{P} = \begin{bmatrix} \boldsymbol{P}_1 & \boldsymbol{P}_1\boldsymbol{E} \\ * & \boldsymbol{P}_0 + \boldsymbol{E}^{\mathrm{T}}\boldsymbol{P}_1\boldsymbol{E} \end{bmatrix} > 0 \tag{15}$$

where $\boldsymbol{P}_1 \in \mathbb{R}^{(n-p)\times(n-p)}$, that satisfies:

$$\boldsymbol{P}\boldsymbol{A}_p + \boldsymbol{A}_p^T\boldsymbol{P} < 0 \tag{16}$$

and ρ is chosen to satisfy:

$$\rho > 2||\boldsymbol{A}_{c21}||(1 + ||\boldsymbol{E}||)\mu_1\beta/\mu_0 + ||\boldsymbol{Q}_{c2}||\beta + \eta_0 \tag{17}$$

where $\mu_0 = -\lambda_{\max}\left(\boldsymbol{P}\boldsymbol{A}_p + \boldsymbol{A}_p^T\boldsymbol{P}\right)$, $\mu_1 = ||\boldsymbol{P}\boldsymbol{Q}_c||$ and η_0 is a small positive real scalar, then the error Equation (12) is driven to the sliding surface in finite time.

Proof: The following Lyapunov function is introduced:

$$V_1(t) = \boldsymbol{e}^T(t)\boldsymbol{P}\boldsymbol{e}(t) \tag{18}$$

The derivative of $V_1(t)$ is given by:

$$\dot{V}_1(t) = \boldsymbol{e}^T(t)(\boldsymbol{P}\boldsymbol{A}_p + \boldsymbol{A}_p^T\boldsymbol{P})\boldsymbol{e}(t) + 2\boldsymbol{e}^T(t)\boldsymbol{P}\boldsymbol{G}_n\boldsymbol{v}(t) - 2\boldsymbol{e}^T\boldsymbol{P}\boldsymbol{Q}_c\xi(t,\boldsymbol{x},\boldsymbol{u}) \tag{19}$$

Note that $\boldsymbol{P}\boldsymbol{G}_n = \boldsymbol{C}_c^T\boldsymbol{P}_0$, and with inequality in Equation (16) and definitions of μ_0 and μ_1, $\dot{V}_1(t)$ becomes:

$$\begin{aligned}\dot{V}_1(t) &\leqslant -\mu_0\left\|\boldsymbol{e}(t)\right\|^2 + 2\boldsymbol{e}_y^T(t)\boldsymbol{P}_0\boldsymbol{v}(t) + 2\left\|\boldsymbol{e}(t)\right\|\mu_1\beta \\ &= \|\boldsymbol{e}(t)\|(-\mu_0\|\boldsymbol{e}(t)\|+2\mu_1\beta) - 2\rho\|\boldsymbol{P}_0\boldsymbol{e}_y(t)\| \\ &\leqslant \|\boldsymbol{e}(t)\|(-\mu_0\|\mathbf{e}(t)\|+2\mu_1\beta)\end{aligned} \tag{20}$$

which shows the magnitude of $\boldsymbol{e}(t)$ decreases when $\|\boldsymbol{e}(t)\| > 2\mu_1\beta/\mu_0$. This implies that in finite time $\|\boldsymbol{e}(t)\|$ will be bounded with respect to the set:

$$\Omega_\varepsilon = \{\boldsymbol{e} : \|\boldsymbol{e}\| < 2\mu_1\beta/\mu_0 + \varepsilon\} \tag{21}$$

where ε is an arbitrary small positive scalar.

In order to prove a sliding motion can be induced on the sliding surface, it's convenient to introduce another change of coordinates to Equation (12) associated with nonsingular matrix:

$$\boldsymbol{T}_E = \begin{bmatrix} \boldsymbol{I}_{n-p} & \boldsymbol{E} \\ \boldsymbol{0} & \boldsymbol{I}_p \end{bmatrix} \tag{22}$$

Applying the change of coordinates $\boldsymbol{T}_E$ yields:

$$\overline{\boldsymbol{A}} = \begin{bmatrix} \overline{\boldsymbol{A}}_{11} & \overline{\boldsymbol{A}}_{12} \\ \overline{\boldsymbol{A}}_{21} & \overline{\boldsymbol{A}}_{22} \end{bmatrix}, \overline{\boldsymbol{C}} = \begin{bmatrix} \boldsymbol{0} & \boldsymbol{I}_p \end{bmatrix}, \overline{\boldsymbol{G}}_n = \begin{bmatrix} \boldsymbol{0} \\ \boldsymbol{I}_p \end{bmatrix}, \overline{\boldsymbol{G}}_l = \begin{bmatrix} \overline{\boldsymbol{G}}_{l1} \\ \overline{\boldsymbol{G}}_{l2} \end{bmatrix}, \overline{\boldsymbol{Q}} = \begin{bmatrix} \overline{\boldsymbol{Q}}_1 \\ \overline{\boldsymbol{Q}}_2 \end{bmatrix} \tag{23}$$

where $\overline{\boldsymbol{A}}_{11} = \boldsymbol{A}_{c11} + \boldsymbol{E}\boldsymbol{A}_{c21}$, $\overline{\boldsymbol{A}}_{21} = \boldsymbol{A}_{c21}$, $\overline{\boldsymbol{Q}}_1 = \boldsymbol{Q}_{c1} + \boldsymbol{E}\boldsymbol{Q}_{c2}$ and $\overline{\boldsymbol{Q}}_2 = \boldsymbol{Q}_{c2}$. The error system in Equation (12) with the change of coordinates $\overline{\boldsymbol{e}} = \boldsymbol{T}_E\boldsymbol{e}$ can be rewritten and partitioned as:

$$\begin{aligned}\dot{\overline{\boldsymbol{e}}}_1(t) &= \overline{\boldsymbol{A}}_{11}\overline{\boldsymbol{e}}_1(t) + (\overline{\boldsymbol{A}}_{12} - \overline{\boldsymbol{G}}_{l1})\overline{\boldsymbol{e}}_y(t) - \overline{\boldsymbol{Q}}_1\xi(t,\boldsymbol{x},\boldsymbol{u}) \\ \dot{\overline{\boldsymbol{e}}}_y(t) &= \overline{\boldsymbol{A}}_{21}\overline{\boldsymbol{e}}_1(t) + (\overline{\boldsymbol{A}}_{22} - \overline{\boldsymbol{G}}_{l2})\overline{\boldsymbol{e}}_y(t) + \boldsymbol{v}(t) - \overline{\boldsymbol{Q}}_2\xi(t,\boldsymbol{x},\boldsymbol{u})\end{aligned} \tag{24}$$

Consider another Lyapunov function candidate $V_2(t) = \overline{\boldsymbol{e}}_y^T(t)\,\boldsymbol{P}_0\overline{\boldsymbol{e}}_y(t)$ where $\boldsymbol{P}_0$ has been defined in Equation (15). The time derivative of $V_2(t)$ along the trajectories of the error system is given by:

$$\begin{aligned}\dot{V}_2(t) &= \dot{\overline{\boldsymbol{e}}}_y^T(t)\boldsymbol{P}_0\overline{\boldsymbol{e}}_y(t) + \overline{\boldsymbol{e}}_y^T(t)\boldsymbol{P}_0\dot{\overline{\boldsymbol{e}}}_y(t) \\ &= \overline{\boldsymbol{e}}_y^T(t)((\overline{\boldsymbol{A}}_{22} - \overline{\boldsymbol{G}}_{l2})^T\boldsymbol{P}_0 + \boldsymbol{P}_0(\overline{\boldsymbol{A}}_{22} - \overline{\boldsymbol{G}}_{l2}))\overline{\boldsymbol{e}}_y(t) \\ &+2\overline{\boldsymbol{e}}_y^T(t)\boldsymbol{P}_0(\overline{\boldsymbol{A}}_{21}\overline{\boldsymbol{e}}_1(t) + \boldsymbol{v}(t) - \overline{\boldsymbol{Q}}_2\xi(t,\boldsymbol{x},\boldsymbol{u}))\end{aligned} \tag{25}$$

Note that:

$$(\boldsymbol{T}_E^{-1})^T\boldsymbol{P}\boldsymbol{T}_E^{-1} = \begin{bmatrix} \boldsymbol{P}_1 & \boldsymbol{0} \\ \boldsymbol{0} & \boldsymbol{P}_0 \end{bmatrix} \tag{26}$$

and:

$$\boldsymbol{T}_E\boldsymbol{A}_p\boldsymbol{T}_E^{-1} = \begin{bmatrix} \overline{\boldsymbol{A}}_{11} & \overline{\boldsymbol{A}}_{12} - \overline{\boldsymbol{G}}_{l1} \\ \overline{\boldsymbol{A}}_{21} & \overline{\boldsymbol{A}}_{22} - \overline{\boldsymbol{G}}_{l2} \end{bmatrix} \tag{27}$$

Combining Equations (16), (26) and (27) yields:

$$(\boldsymbol{T}_E^{-1})^T(\boldsymbol{P}\boldsymbol{A}_p + \boldsymbol{A}_p^T\boldsymbol{P})\boldsymbol{T}_E^{-1} = \begin{bmatrix} \boldsymbol{P}_1\overline{\boldsymbol{A}}_{11} + \overline{\boldsymbol{A}}_{11}^T\boldsymbol{P}_1 & \boldsymbol{N}_1 \\ \boldsymbol{N}_2 & \boldsymbol{P}_0(\overline{\boldsymbol{A}}_{22} - \overline{\boldsymbol{G}}_{l2}) + (\overline{\boldsymbol{A}}_{22} - \overline{\boldsymbol{G}}_{l2})^T\boldsymbol{P}_0 \end{bmatrix} < 0 \quad (28)$$

where $\boldsymbol{N}_1$ and $\boldsymbol{N}_2$ are elements that are not necessary in the following analysis. Since Equation (28) is symmetric, it is obvious that:

$$\boldsymbol{P}_0(\overline{\boldsymbol{A}}_{22} - \overline{\boldsymbol{G}}_{l2}) + (\overline{\boldsymbol{A}}_{22} - \overline{\boldsymbol{G}}_{l2})^T\boldsymbol{P}_0 < 0 \quad (29)$$

therefore from Equations (25) and (29) it follows that:

$$\dot{V}_2(t) \leqslant 2\overline{\boldsymbol{e}}_y^T(t)\boldsymbol{P}_0(\overline{\boldsymbol{A}}_{21}\overline{\boldsymbol{e}}_1(t) + \boldsymbol{\nu}(t) - \overline{\boldsymbol{Q}}_2\xi(t,\boldsymbol{x},\boldsymbol{u})) \quad (30)$$

Since $\overline{\boldsymbol{e}}_1(t) = \boldsymbol{e}_1(t) + \boldsymbol{E}\boldsymbol{e}_y(t)$, considering Equation (21) yields:

$$||\overline{\boldsymbol{e}}_1(t)|| < ||\boldsymbol{e}_1(t)|| + ||\boldsymbol{E}||\,||\boldsymbol{e}_y(t)|| < (1 + ||\boldsymbol{E}||)(2\mu_1\beta/\mu_0 + \varepsilon) \quad (31)$$

then we combine Equations (30) and (31) to get:

$$\begin{aligned} \dot{V}_2(t) \quad &\leqslant 2\big|\big|\boldsymbol{P}_0\overline{\boldsymbol{e}}_y(t)\big|\big|(2\big|\big|\overline{\boldsymbol{A}}_{21}\big|\big|(1+\big|\big|\boldsymbol{E}\big|\big|)\mu_1\beta/\mu_0+\big|\big|\overline{\boldsymbol{Q}}_2\big|\big|\beta) \\ &-2\rho(\boldsymbol{P}_0\overline{\boldsymbol{e}}_y(t))^T\frac{\boldsymbol{P}_0\overline{\boldsymbol{e}}_y(t)}{||\boldsymbol{P}_0\overline{\boldsymbol{e}}_y(t)||} \\ &\leqslant -2\big|\big|\boldsymbol{P}_0\overline{\boldsymbol{e}}_y(t)\big|\big|(\rho - 2\big|\big|\overline{\boldsymbol{A}}_{21}\big|\big|(1+\big|\big|\boldsymbol{E}\big|\big|)\mu_1\beta/\mu_0-\big|\big|\overline{\boldsymbol{Q}}_2\big|\big|\beta) \end{aligned} \quad (32)$$

Note that $\overline{\boldsymbol{A}}_{21} = \boldsymbol{A}_{c21}$ and $\overline{\boldsymbol{Q}}_2 = \boldsymbol{Q}_{c2}$. Then, substituting Equation (17) into Equation (32) yields:

$$\dot{V}_2(t) < 0 \quad (33)$$

which means the reachability condition is satisfied, and a sliding motion on S is attained in finite time. Thus **Theorem 1** is proved.

Once the sliding mode surface is reached, which indicates $\dot{\boldsymbol{e}}_y = \boldsymbol{e}_y = 0$. Note that $\boldsymbol{A}_{p11} = \boldsymbol{A}_{c11}$ and $\boldsymbol{A}_{p21} = \boldsymbol{A}_{c21}$, the error system in Equation (13) can be simplified as:

$$\begin{aligned} \dot{\boldsymbol{e}}_1(t) &= \boldsymbol{A}_{c11}\boldsymbol{e}_1(t) - \boldsymbol{E}\boldsymbol{v}_{\mathrm{eq}}(t) - \boldsymbol{Q}_{c1}\xi(t,\boldsymbol{x},\boldsymbol{u}) \\ 0 &= \boldsymbol{A}_{c21}\boldsymbol{e}_1(t) + \boldsymbol{v}_{\mathrm{eq}}(t) - \boldsymbol{Q}_{c2}\xi(t,\boldsymbol{x},\boldsymbol{u}) \end{aligned} \quad (34)$$

where $\boldsymbol{v}_{\mathrm{eq}}(t)$ is the so-called equivalent output error injection term, which represent the average behavior of the discontinuous term $\boldsymbol{v}(t)$ and can be obtained by a low pass filter from $\boldsymbol{v}(t)$. Eliminating $\boldsymbol{v}_{\mathrm{eq}}(t)$ from Equation (34) yields a reduced order system:

$$\dot{\boldsymbol{e}}_1(t) = (\boldsymbol{A}_{c11} + \boldsymbol{E}\boldsymbol{A}_{c21})\boldsymbol{e}_1(t) - (\boldsymbol{Q}_{c1} + \boldsymbol{E}\boldsymbol{Q}_{c2})\xi(t,\boldsymbol{x},\boldsymbol{u}) \quad (35)$$

Assume that $\boldsymbol{Q}_c$ is in the structure:

$$\boldsymbol{Q}_c = \begin{bmatrix} -\boldsymbol{E}\boldsymbol{X} \\ \boldsymbol{X} \end{bmatrix} \quad (36)$$

where $\boldsymbol{X} \in \mathbb{R}^{p\times h}$ is an arbitrary real matrix. The structure of $\boldsymbol{Q}_c$ indicates $\boldsymbol{Q}_c$ satisfies $\boldsymbol{Q}_c = \boldsymbol{G}_n\boldsymbol{X}$ for some $\boldsymbol{X} \in \mathbb{R}^{p\times h}$. Combining Equations (35) and (36) yields:

$$\dot{\boldsymbol{e}}_1(t) = (\boldsymbol{A}_{c11} + \boldsymbol{E}\boldsymbol{A}_{c21})\boldsymbol{e}_1(t) \quad (37)$$

This is an ideal sliding motion which is entirely independent of $\xi(t, \boldsymbol{x}, \boldsymbol{u})$. The remaining dynamics $\boldsymbol{e}_1(t)$ is governed by $(\boldsymbol{A}_{p11} + \boldsymbol{E}\boldsymbol{A}_{p21})$. From Equation (28) it can be shown that $\boldsymbol{P}_1(\boldsymbol{A}_{c11} + \boldsymbol{E}\boldsymbol{A}_{c21}) + (\boldsymbol{A}_{c11} + \boldsymbol{E}\boldsymbol{A}_{c21})^T\boldsymbol{P}_1 < 0$ and $\boldsymbol{P}_1 > 0$, thus the matrix $(\boldsymbol{A}_{c11} + \boldsymbol{E}\boldsymbol{A}_{c21})$ is stable, which means the reduced order motion can be maintained on the sliding surface. Notice that for the existence of an ideal sliding motion, the match condition Equation (36) is not required, and a large enough ρ is sufficient to induce a sliding motion, like Equation (17). The match condition is only required for the reduced sliding motion Equation (35) to be independent of $\xi(t, \boldsymbol{x}, \boldsymbol{u})$.

The design philosophy is to synthesize $\boldsymbol{P}$ and $\boldsymbol{G}_l$ so that inequality Equation (16) can be achieved. The design method adopted is to use linear matrix inequalities (LMIs) [17–19]. Here $\boldsymbol{P}$ and $\boldsymbol{G}_l$ will be chosen so that the inequality:

$$\boldsymbol{P}\boldsymbol{A}_p + \boldsymbol{A}_p^T\boldsymbol{P} < -\boldsymbol{P}\boldsymbol{W}\boldsymbol{P} - \boldsymbol{P}\boldsymbol{G}_l\boldsymbol{V}\boldsymbol{G}_l^T\boldsymbol{P} \tag{38}$$

is satisfied, where the design weighting matrices $\boldsymbol{W}$ and $\boldsymbol{V}$ are diagonal positive definite, and $\boldsymbol{P}$ has the structure in Equation (15). Let $\boldsymbol{Z} = \boldsymbol{P}\boldsymbol{G}_l$ and substituting $\boldsymbol{A}_c - \boldsymbol{G}_l\boldsymbol{C}_c$ for $\boldsymbol{A}_p$, the inequality can be written as:

$$\boldsymbol{P}\boldsymbol{A}_c + \boldsymbol{A}_c^T\boldsymbol{P} + (\boldsymbol{Z}^T - \boldsymbol{V}^{-1}\boldsymbol{C}_c)^T\boldsymbol{V}(\boldsymbol{Z}^T - \boldsymbol{V}^{-1}\boldsymbol{C}_c) - \boldsymbol{C}_c^T\boldsymbol{V}^{-1}\boldsymbol{C}_c + \boldsymbol{P}\boldsymbol{W}\boldsymbol{P} < 0 \tag{39}$$

Choosing:

$$\boldsymbol{Z}^T = \boldsymbol{V}^{-1}\boldsymbol{C}_c \tag{40}$$

to eliminate the third term in Equation (39) yields:

$$\boldsymbol{P}\boldsymbol{A}_p + \boldsymbol{A}_p^T\boldsymbol{P} - \boldsymbol{C}_c^T\boldsymbol{V}^{-1}\boldsymbol{C}_c + \boldsymbol{P}\boldsymbol{W}\boldsymbol{P} < 0 \tag{41}$$

Thus the inequality Equation (16) is replaced by Equation (41), which is required to be satisfied. From Equation (40) $\boldsymbol{G}_l$ can be directly calculated as:

$$\boldsymbol{G}_l = \boldsymbol{P}^{-1}\boldsymbol{C}_c^T\boldsymbol{V}^{-1} \tag{42}$$

From the structure of $\boldsymbol{G}_l$ it can be shown that the "magnitude" of $\boldsymbol{G}_l$ is directly determined by the "magnitude" of $\boldsymbol{P}^{-1}$, and the larger $\boldsymbol{G}_l$ is, the more difficult it can be realized in hardware. The target considered here is to minimize $trace(\boldsymbol{P}^{-1})$ subject to $\boldsymbol{P}$ satisfying Equation (41). In fact the motivation here is to seek optimal value of linear gain $\boldsymbol{G}_l$ by the standard linear quadratic Gausssian (LQG) optimal observer design method, as described in [20]. The associated optimal cost is given by $trace(\boldsymbol{P}^{-1})$. The method can be summarized as:

- minimize $trace(\boldsymbol{S})$ with regard to $\boldsymbol{P}_1$, $\boldsymbol{P}_0$, $\boldsymbol{E}$ and $\boldsymbol{S}$ subject to:

$$\boldsymbol{P} = \begin{bmatrix} \boldsymbol{P}_1 & \boldsymbol{P}_1\boldsymbol{E} \\ * & \boldsymbol{P}_0 + \boldsymbol{E}^T\boldsymbol{P}_1\boldsymbol{E} \end{bmatrix} > 0 \tag{43}$$

$$\begin{bmatrix} \boldsymbol{P}\boldsymbol{A}_c + \boldsymbol{A}_c^T\boldsymbol{P} - \boldsymbol{C}_c\boldsymbol{V}^{-1}\boldsymbol{C}_c & \boldsymbol{P} \\ * & -\boldsymbol{W}^{-1} \end{bmatrix} < 0 \tag{44}$$

$$\begin{bmatrix} -\boldsymbol{P} & \boldsymbol{I}_n \\ * & -\boldsymbol{S} \end{bmatrix} < 0 \tag{45}$$

where $\boldsymbol{S} \in \mathbb{R}^{n\times n}$ is symmetric positive definite. This represents a convex optimization problem, which can be handled by standard LMI software. Then $\boldsymbol{G}_n$ and $\boldsymbol{v}(t)$ can be both obtained with E and $\boldsymbol{P}_0$.

A new architecture for estimating engine performance deterioration is described based on the SMO designed above. A two-spool turbofan engine is considered in this paper, of which the schematic model is shown in Figure 1. The airflow is supplied by a single inlet. Airflow passes through the fan and separates into two streams: one passes through engine core path, and the other passes through

the bypass duct. Fuel is injected in the combustor and burned to produce the hot gas to drive the turbines. The fan and low pressure compressor (LPC) are driven by low pressure turbine (LPT), while high pressure compressor (HPC) is driven by high pressure turbine (HPT). The airflow leaves through the nozzle, which has a variable cross section area A_8. The notations used in this paper and their descriptions are shown in Notations Section.

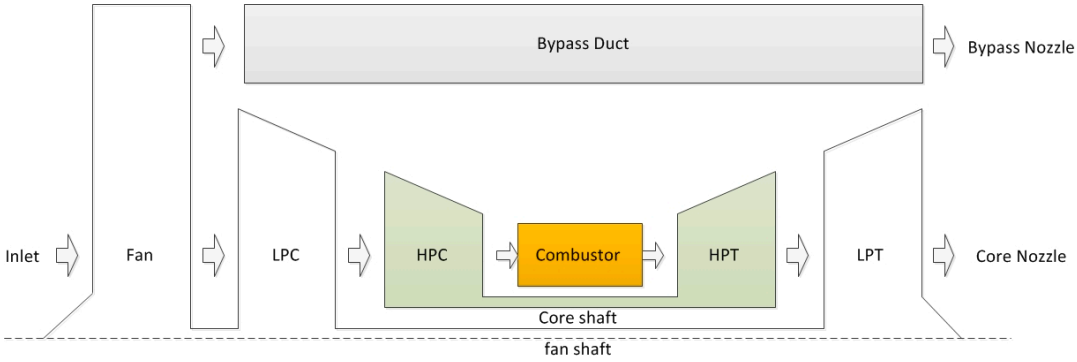

Figure 1. Schematic model of a two-spool turbofan engine.

As engine parts wear from regular operation, the lifespan of components will be reduced. The aging of components is reflected as changes in internal flow capacities and component efficiencies, and components' sudden damages also result in the change of component performance and characteristics. Thus these capacities and efficiencies of components are chosen as "health parameters" to reflect component health performance. The degradations of health parameters are described as:

$$\Delta h_i = \frac{h_i}{h_{i,r}} - 1 \quad i = 1, 2, .., 8 \tag{46}$$

where $h_{i,r}$ denotes the nominal value of h_i. A normalized health parameter varies between 0 and 1, with 1 representing a healthy component and 0 a "fully deteriorated" one. The maximum level of deterioration indicates an engine overhaul is necessary. The health parameters are employed to handle with both slowly aging and sudden fault. The purpose of a gas-path health monitoring (GPHM) system is to estimate these health parameters for performance monitoring and fault detection.

Mechanical system dynamics due to rotating inertias constitute the most important contribution to engine transient behavior [21]. Thus rotating dynamics are the most important dynamics to be considered. In view of this, $\boldsymbol{x}$ is chosen as $col(N_{\mathrm{L}}, N_{\mathrm{H}})$. Newton's law for rotating masses is applied to each shaft as:

$$\begin{aligned} \dot{N}_{\mathrm{L}} &= f_1(N_{\mathrm{L}}, N_{\mathrm{H}}, \boldsymbol{u}, \boldsymbol{v}, \boldsymbol{h}) \\ \dot{N}_{\mathrm{H}} &= f_2(N_{\mathrm{L}}, N_{\mathrm{H}}, \boldsymbol{u}, \boldsymbol{v}, \boldsymbol{h}) \end{aligned} \tag{47}$$

where f_1 and f_2 are the net torques delivered by LPT and HPT. $\boldsymbol{u}$ contains the control input components, which is given by $col(W_{\mathrm{f}}, A_8)$, and $\boldsymbol{v}$ denotes the external parameters (flight condition). Because of the intricate geometry of the engine components and the complexity of airflow, algebraic expressions for f_1 and f_2 are unavailable. A practical modeling approach is the piecewise linear SVM. Employing perturbation techniques at each equilibrium condition, a set of linear relationships which depict the interactions of the engine states with inputs and outputs are established, as described in Equation (1). Compared to the nonlinear CLM, SVM takes a smaller computation burden and is more feasible in real-time applications.

Most of sensors used to conduct GPHM are installed on the engine for control purposes, and some of these sensors are employed to enable GPHM system. In this paper the available measurements are defined by the standard suite of sensors found in the tactical turbofan engine control system. The output vector is chosen as $col(N_{\mathrm{L}}, N_{\mathrm{H}}, T_{25}, P_{25}, T_3, P_3, EGT)$. Given this sensor suite constraint,

observability studies indicate seven health parameters could be discerned properly. Table 1 lists the statistical data of engine deterioration level for certain flight cycles. Compared to other health parameters, the flow capacity of LPT deteriorates much less, so it should then be ignored. Thus the health parameters monitored are given by $col(h_1, h_2, h_3, h_4, h_5, h_6, h_7)$.

Table 1. The variation of health parameters with different flight cycles (%).

Cycle Number	h_1	h_2	h_3	h_4	h_5	h_6	h_7	h_8
3000	−1.46	−2.08	−2.94	−3.91	−2.63	1.76	−0.53	0.26
4500	−2.04	−3.04	−6.17	−8.99	−3.22	2.17	−0.81	0.34
6000	−2.61	−4.00	−9.40	−14.06	−3.81	2.57	−1.11	0.42

Since health parameters are augmented as state variables, as described in Equation (2), the estimation of component degradation can be easily obtained by the described SMO. The proposed GPHM architecture is shown in Figure 2.

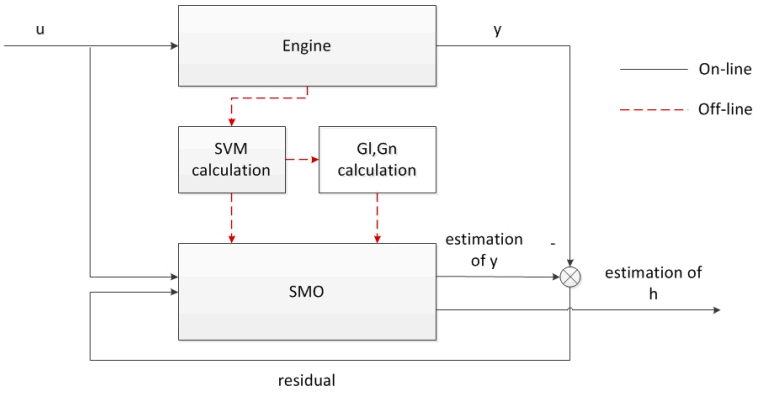

Figure 2. Schematic representation of gas-path health monitoring (GPHM).

Due to the SVM of the turbofan engine being time-invariant, the gain matrix of the SMO can be computed off-line. Once the SMO is well designed, it enables the GPHM system to monitor the components' performance in real-time for in-flight health tracking. The SMO possesses a strong robustness against a class of uncertainties, which is precious to the estimation of aero-engine health parameter problem, considering the inevitable modeling error from linearizing process of an aircraft engine.

3. Results and Discussion

In this paper, a CLM introduced in [3], which captures the nonlinear behavior of a twin-spool turbofan engine with highly fidelity is considered, working as a simulation platform for a real engine. The CLM consists of a set of individual components, each of which requires a number of inputs and generates one or more variables. The steady state simulation of CLM is based on mass flow balance and power balance equations, while the transient simulation, initialed by steady state calculation, follows mass flow balance and rotor dynamics equations. The Newton-Raphson method is employed to solve the nonlinear expressions both in steady state case and transient dynamics. Iterative solution of nonlinear equations in each step stops once the iteration number reaches 10, or the iteration error is less than 0.01. The CLM is written using C language and packaged with dynamic link library (DLL) for use in the Matlab environment [22,23]. The health parameters are modeled and health degrading injection is available in the CLM. Sensor dynamics are ignored in the simulations, with the assumption that they have high enough bandwidth. The model has been validated versus the testing data. The engine is simulated at the reference flight condition and at a nominal cruise power setting,

and the effectiveness of the proposed health estimation approach will be demonstrated by using the simulated data extracted from the CLM.

The positive scalar ρ is a critical parameter to be determined. In fact, ρ provides a degree of freedom in terms of the trade-off between robustness and chattering. The greater the value of ρ, a stronger robustness is present to ensure sliding mode occurrence, but a higher chattering problem follows. Assume that $\beta = 1.0$, from Equation (17) it can be calculated that ρ is required to satisfy $\rho > 0.0092$. In this paper ρ is set to 0.01. $\boldsymbol{W}$ and $\boldsymbol{V}$ are user-defined matrices and specify $\boldsymbol{W} = \boldsymbol{I}_9$ and $\boldsymbol{V} = \boldsymbol{L}_7$. Considering aero-engines are prone to noises, the nominal white Gaussian noises are introduced to the measurements. The standard deviation of noises is given by $\sigma_{\text{noise}} = 0.0015$, which is determined by practical experience.

3.1. Single Health Parameter Degradation Case

In this case (Case 1) a −5% abrupt shift is imposed on h_5 from its normal value, to simulate a typical fault scenario in engine real operations. When engines are operated near the stall limit, the steady axisymmetric flow pattern in LPC becomes unstable. This instability may cause the phenomenon of surge and rotating stall in LPC, which are generally reflected by h_5 degradation. In order to testify the robustness of SMO, the modeling uncertainty term $\boldsymbol{Q}_c \boldsymbol{\xi}(t, \boldsymbol{x}, \boldsymbol{u})$ is introduced here. In the simulation specify $\boldsymbol{Q}_c = \boldsymbol{G}_n$ to satisfy matching condition. Assume that the modeling mismatches are in system matrix $\boldsymbol{A}_c$, then $\boldsymbol{\xi}(t, \boldsymbol{x}, \boldsymbol{u})$ is given by:

$$\xi = \begin{bmatrix} 0.13 & 0.04 & 0.03 & 0.11 & 0.09 & 0.06 & 0.18 & 0.03 & 0.05 \\ 0.30 & 0.02 & 0.01 & 0.05 & 0.04 & 0.05 & 0.10 & 0.07 & 0.02 \\ 0.10 & 0.04 & 0.01 & 0.10 & 0.02 & 0.02 & 0.07 & 0.03 & 0.01 \\ 0.02 & 0.02 & 0.03 & 0.09 & 0.04 & 0.04 & 0.02 & 0.03 & 0.02 \\ 0.11 & 0.05 & 0.06 & 0.01 & 0.07 & 0.16 & 0.10 & 0.03 & 0.07 \\ 0.02 & 0.03 & 0.03 & 0.14 & 0.09 & 0.04 & 0.08 & 0.03 & 0.09 \\ 0.01 & 0.14 & 0.12 & 0.01 & 0.02 & 0.06 & 0.12 & 0.06 & 0.04 \end{bmatrix} \boldsymbol{x}_c \quad (48)$$

The health parameter estimation results are shown in Figure 3a. The output errors between the engine and the observer are shown in Figure 3b, which indicates the sliding mode is quickly achieved soon after the malfunction occurs. The degraded heath parameter is estimated with acceptable errors as shown in Figure 3c. The maximum root-mean square error (RMSE) between the real values and the estimated ones is shown in Table 2. The diagnosing time is defined as the time when estimated values catch up with real values after fault injection. The diagnosing time is shown in Table 3.

Table 2. The maximum root-mean square error (RMSE) (%).

Methods	Case 1		Case 2
	Matched Q_c	Unmatched Q_c	Matched Q_c
SMO	0.45	0.50	0.34
KF	0.87	1.45	0.67

Table 3. The diagnosis time (s).

Methods	Case 1		Case 2
	Matched Q_c	Unmatched Q_c	Matched Q_c
SMO	0.67	1.21	0.61
KF	3.71	4.55	3.52

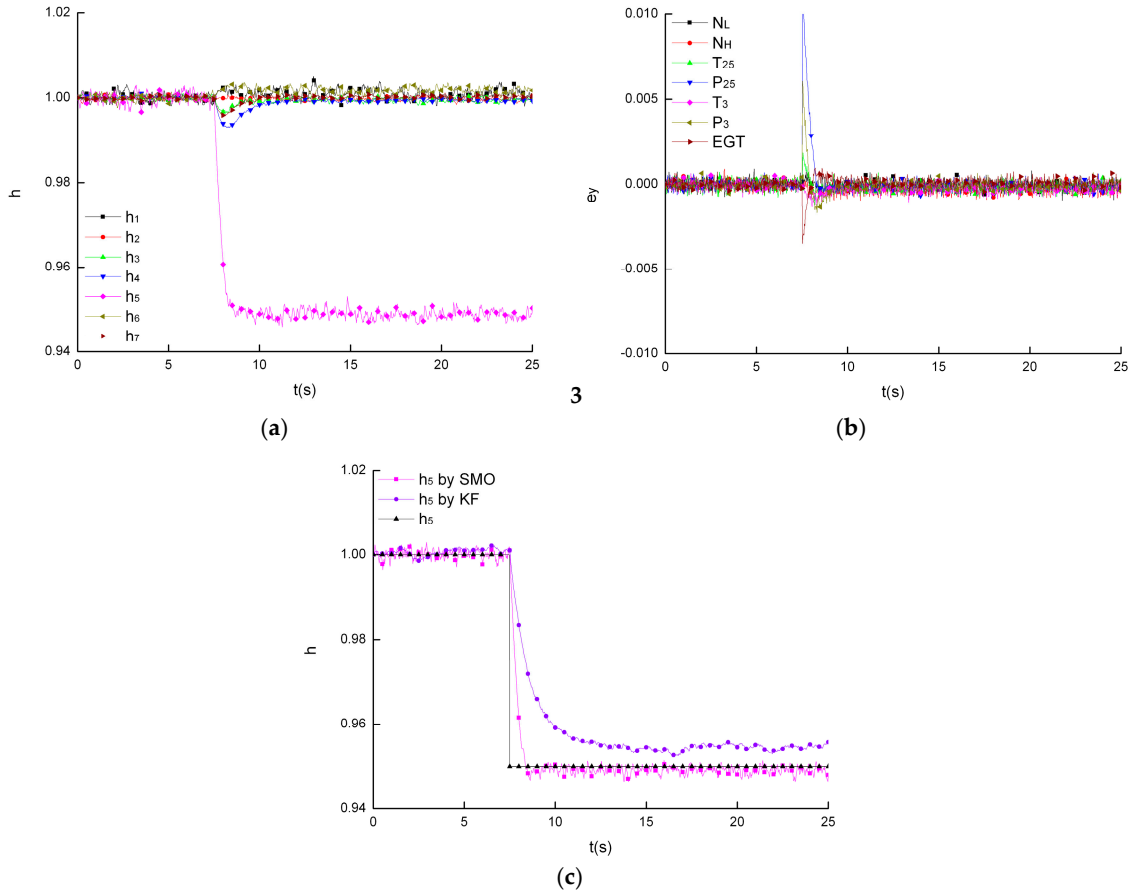

Figure 3. Single health parameter degradation (matched uncertainties): (**a**) estimation of health parameters by sliding mode observer (SMO); (**b**) errors between y and $\hat{y}$ by SMO; and (**c**) degraded parameter estimation by KF and SMO.

In order to show the advantage of the developed SMO in robustness, the same degrading problem is introduced to the nominal KF based monitoring system with the same model uncertainties. The results are also shown in Figure 3c, Tables 2 and 3. It can be seen that the estimation of h_5 is inaccurate due to the uncertainties, which emphasizes the advantage of the SMO in robustness against uncertainties.

As mentioned above, the matching condition for $\boldsymbol{Q}_c$ is not necessary for the existence of an ideal sliding motion, which a large enough ρ is sufficient to induce. The match condition is only required for the reduced sliding motion to be independent of $\boldsymbol{\xi}(t, \boldsymbol{x}, \boldsymbol{u})$. Here an unmatched $\boldsymbol{Q}_c$ is introduced to the system in the same degrading problem mentioned above. $\boldsymbol{Q}_c$ is specified to be:

$$\boldsymbol{Q}_c = \begin{bmatrix} \boldsymbol{0} \\ \boldsymbol{I}_p \end{bmatrix} \tag{49}$$

and $\boldsymbol{\xi}(t, \boldsymbol{x}, \boldsymbol{u})$ is identical to that in Equation (47). The degradation problem is handled by the SMO framework and the KF framework, respectively. Figure 4 depicts the health estimation, in the case of unmatched uncertainties, via the SMO and the KF approaches. As can be seen from Figure 4a, the degraded health parameter can be found and tracked, with an accuracy of about 95% by the SMO, and other health parameters drift slightly from their nominal values after the degradation begins. This indicates that though $\boldsymbol{Q}_c$ does not satisfy Equation (36), the sliding motion is still attained. The estimation results, however, are polluted by uncertainties. In comparison, the KF framework performs a poorer quality in handling the same degrading problem, as shown in Figure 4b.

The degraded health parameter is estimated with an undesirable error, and other health parameters drift away after the degrading injection. The simulation confirms that the described SMO is designed to be stable regardless of the form of $\boldsymbol{Q}_c$. Figure 4c,d show the output errors in the SMO and the KF respectively. $\boldsymbol{e}_y$ of the SMO can converge to zero quickly after the degradation occurs, as shown in Figure 4c, while $\boldsymbol{e}_y$ of the KF is divergent as shown in Figure 4d. The maximum RMSE values of both frameworks are shown in Table 2 and the diagnosis time in Table 3.

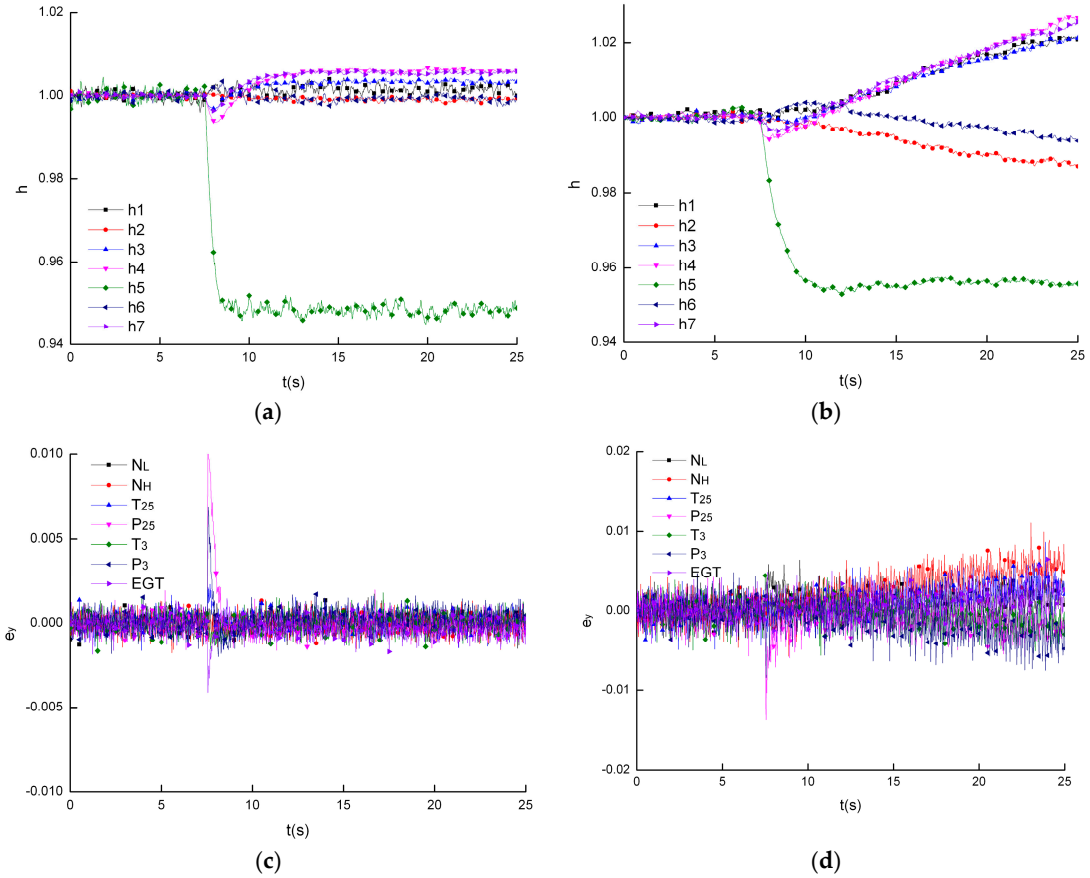

Figure 4. Single health parameter degradation (unmatched uncertainties): (**a**) estimation of health parameters by SMO; (**b**) estimation of health parameters by KF; (**c**) errors between y and $\hat{y}$ by SMO; and (**d**) errors between y and $\hat{y}$ by KF.

3.2. Multi Health Parameter Degradation Case

In this case (Case 2), the multi health degradation problem is tested through the proposed scheme, with both bias and drift degradations involved. In this scenario, h_5 abruptly drops to 96% of the normal condition, while h_1 drifts to 98% and h_7 drifts to 102% in 5 s (flow capacity of turbines rises in degrading cases). The matched uncertainty term $\boldsymbol{Q}_c\boldsymbol{\xi}(t, \boldsymbol{x}, \boldsymbol{u})$ is considered here, which is the same as that in the first simulation of Case 1.

The malfunctions are estimated accurately by the proposed approach, as shown in Figure 5a. Figure 5b shows the output errors. The same problem is introduced to the KF-based scheme, and comparisons are shown in Figure 5c. Results indicate that the developed SMO is able to handle multi-fault cases with model mismatches, while in the simulation of the KF-based scheme, the faulty health parameters fail to be tracked correctly. The maximum RMSE values of both schemes are shown in Table 2 and the diagnosis time in Table 3.

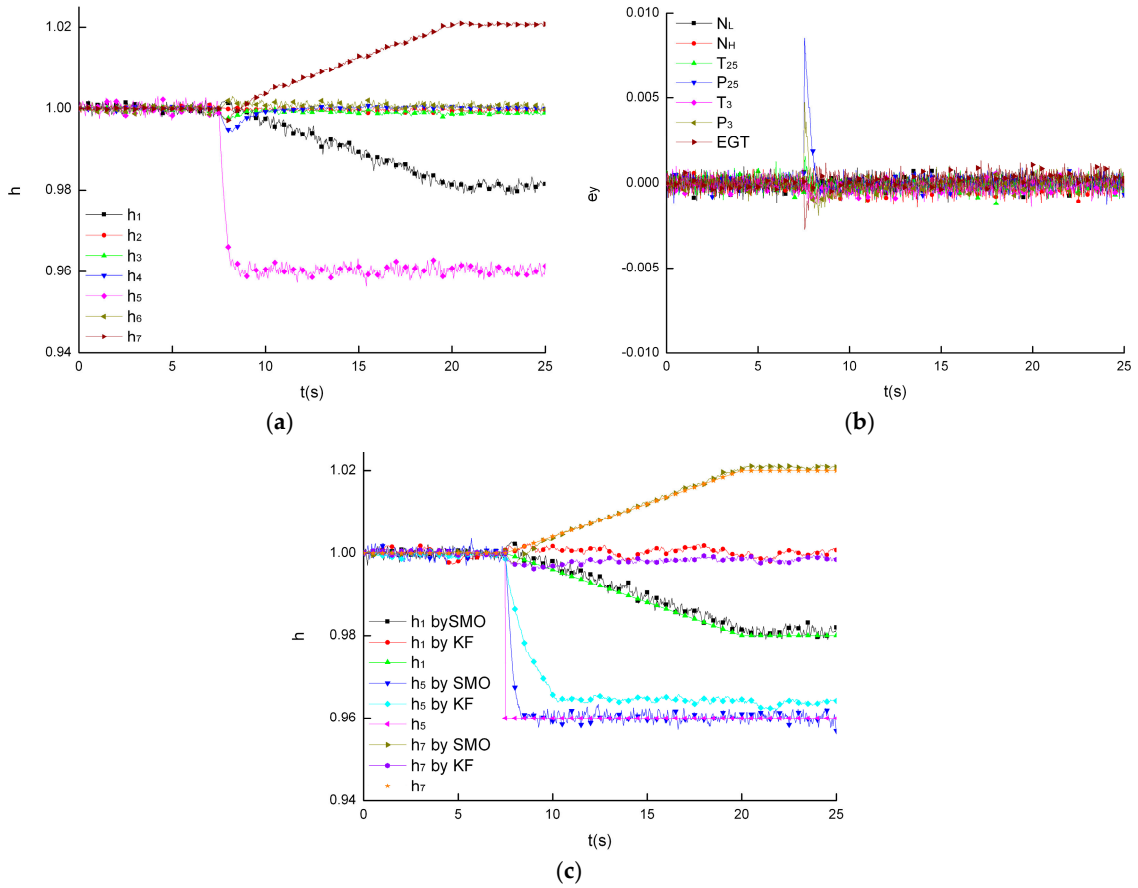

Figure 5. Multi health parameter degradations (matched uncertainties): (**a**) estimation of health parameters by SMO; (**b**) errors between y and $\hat{y}$ by SMO; and (**c**) degraded parameters estimation by KF and SMO.

4. Conclusions

A SMO-based health monitoring system for an aircraft turbofan engine has been developed in this paper. With health parameters regarded as state variables, the estimation of degradation is in fact a matter of state observation. The convergence of the error system in uncertainty-existing circumstances is demonstrated, and a robust SMO has been described aiming at estimating the degradations of health parameters in engine gas-path, where the modeling uncertainties are considered. A set of simulations have been conducted on the CLM, and a comparison to the traditional KF-based health monitoring system has proven the ascendency of the proposed SMO. Results have shown a range of degradation cases can be faithfully detected and estimated with suitable accuracy and quick diagnosis speed by the described observer.

Acknowledgments: We are grateful for the financial support of the National Nature Science Foundation of China (No. 51276087) and Jiangsu Province Nature Science Foundation (No. BK20130802).

Author Contributions: Xiaodong Chang and Jinquan Huang conceived and designed the algorithm; Feng Lu and Xiaodong Chang wrote the program and performed the simulations; Jinquan Huang and Haobo Sun analyzed the data; Xiaodong Chang wrote the paper.

Conflicts of Interest: The authors declare no conflict of interest. The founding sponsors had no role in the design of the study; in the collection, analyses, or interpretation of data; in the writing of the manuscript, and in the decision to publish the results.

Notations

LPC	Low pressure compressor
HPC	High pressure compressor
HPT	High pressure turbine
LPT	Low pressure turbine
N_L	Low pressure rotor speed
N_H	High pressure rotor speed
$\boldsymbol{h}$	Health parameter vector
h_1	LPC efficiency
h_2	HPC efficiency
h_3	HPT efficiency
h_4	LPT efficiency
h_5	LPC flow capacity
h_6	HPC flow capacity
h_7	HPT flow capacity
h_8	LPT flow capacity
W_f	Fuel flow rate
A_8	Nozzle area
P_{25}	HPC inlet pressure
T_{25}	HPC inlet temperature
P_3	Combustor inlet pressure
T_3	Combustor inlet temperature
EGT	Outlet temperature of 1st stage inlet guide vane of LPT

References

1. Simon, D.L. *An Integrated Architecture for on-Board Aircraft Engine Performance Trend Monitoring and Gas Path Fault Diagnostics*; National Aeronautics and Space Administration: Cleveland, OH, USA, 2010.
2. Armstrong, J.B.; Simon, D.L. *Implementation of an Integrated On-Board Aircraft Engine Diagnostic Architecture*; National Aeronautics and Space Administration: Cleveland, OH, USA, 2012.
3. Lu, F.; Huang, J.; Lv, Y. Gas path health monitoring for a turbofan engine based on a nonlinear filtering approach. *Energies* **2013**, *6*, 492–513. [CrossRef]
4. Luppold, R.H.; Roman, J.R.; Gallops, G.W.; Kerr, L.J. Estimating in-flight engine performance variations using Kalman filter concepts. In Proceedings of the 25th Joint Propulsion Conference, Monterey, CA, USA, 10–13 July 1989.
5. Simon, D.; Simon, D.L. Constrained Kalman filtering via density function truncation for turbofan engine health estimation. *Int. J. Syst. Sci.* **2010**, *41*, 159–171. [CrossRef]
6. Brotherton, T.; Volponi, A.; Luppold, R.; Simon, D.L. eSTORM: Enhanced self tuning on-board real-time engine model. In Proceedings of the 2003 IEEE Aerospace Conference, Big Sky, MT, USA, 8–15 March 2003; pp. 3075–3086.
7. Volponi, A.; Simon, D.L. *Enhanced Self Tuning on-Board Real-Time Model (eSTORM) for Aircraft Engine Performance Health Tracking*; Pratt and Whitney Aircraft Group: East Hartford, CT, USA, 2008.
8. Edwards, C.; Spurgeon, S.K.; Patton, R.J. Sliding mode observers for fault detection and isolation. *Automatica* **2000**, *36*, 541–553. [CrossRef]
9. Ng, K.Y.; Tan, C.P.; Oetomo, D. Disturbance decoupled fault reconstruction using cascaded sliding mode observers. *Automatica* **2012**, *48*, 794–799. [CrossRef]
10. Tan, C.P.; Edwards, C. Sliding mode observers for detection and reconstruction of sensor faults. *Automatica* **2002**, *38*, 1815–1821. [CrossRef]
11. Alwi, H.; Edwards, C. Development and application of sliding mode LPV fault reconstruction schemes for the ADDSAFE Benchmark. *Control Eng. Pract.* **2014**, *31*, 148–170. [CrossRef]

12. Rahme, S.; Meskin, N. Adaptive sliding mode observer for sensor fault diagnosis of an industrial gas turbine. *Control Eng. Pract.* **2015**, *38*, 57–74. [CrossRef]
13. Sugiyama, N. Derivation of system matrices from nonlinear dynamic simulation of jet engines. *J. Guid. Control Dyn.* **1994**, *17*, 1320–1326. [CrossRef]
14. Feng, Z.; Sun, J.; Huang, J.; Cai, H. A new method for establishing a state variable of aeroengine. *J. Aerosp. Power* **1998**, *13*, 435–438.
15. Zhang, P. Aeroengine Fault Diagnostics Based on Kalman Filter. Ph.D. Thesis, Nanjing University of Aeronautics and Astronautics, Nanjing, China, 2008. (In Chinese)
16. Lin, Y.H.; Zhang, H.B. Establishment of State Variable Model of Aeroengine with Improved Least Square Fitting. *Appl. Mech. Mater.* **2010**, *40–41*, 27–33. [CrossRef]
17. Tan, C.P.; Edwards, C. An LMI approach for designing sliding mode observers. *Int. J. Control* **2001**, *74*, 1559–1568. [CrossRef]
18. Edwards, C. A practical method for the design of sliding mode controllers using linear matrix inequalities. *Automatica* **2004**, *40*, 1761–1769. [CrossRef]
19. El Ghaoui, L.; Feron, E.; Balakrishnan, V. *Linear Matrix Inequalities in System and Control Theory*; Society for Industrial and Applied Mathematics: Philadelphia, PA, USA, 1994.
20. Maciejowski, J.M. *Multivariable Feedback Design (Electronic Systems Engineering Series)*; Addison-Wesley: Wokingham, UK, 1989.
21. Richer, H. *Advanced Control of Turbofan Engines*; Springer Science & Business Media: New York, NY, USA, 2011; Volume 377, pp. 51–55.
22. Zhou, W. Research on Object-Oriented Modeling and Simulation for Aeroengine and Control System. Ph.D. Thesis, Nanjing University of Aeronautics and Astronautics, Nanjing, China, 2006. (In Chinese)
23. Lu, F.; Huang, J. Engine Component Performance Prognostics Based on Decision Fusion. *Acta Aeronaut. Sin.* **2009**, *30*, 1795–1800.